Received: 7 June 2021 | Revised: 13 August 2021 | Accepted: 16 August 2021

DOI: 10.1002/glia.24080

GLIA

WILEY

RESEARCH ARTICLE

Urokinase plasminogen activator mediates changes in human astrocytes modeling fragile X syndrome

Ulla-Kaisa Peteri[1] | Juho Pitkonen[1] | Ilario de Toma[2] | Otso Nieminen[1] | Kagistia Hana Utami[3] | Tomas M. Strandin[4] | Padraic Corcoran[5] | Laurent Roybon[6] | Antti Vaheri[4] | Iryna Ethell[7] | Plinio Casarotto[8] | Mahmoud A. Pouladi[3,9] | Maija L. Castrén[1]

[1]Department of Physiology, Faculty of Medicine, University of Helsinki, Helsinki, Finland

[2]Systems Neurobiology Laboratory, Barcelona Institute of Science and Technology, Barcelona, Spain

[3]Department of Physiology, National University of Singapore (NUS), Singapore, Singapore

[4]Department of Virology, Faculty of Medicine, University of Helsinki, Helsinki, Finland

[5]Array and Analysis Facility, Department of Medical Sciences, Uppsala University, Uppsala, Sweden

[6]iPSC Laboratory for CNS Disease Modeling, Department of Experimental Medical Science, BMC D10, and MultiPark and the Lund Stem Cell Center, Lund University, Lund, Sweden

[7]Biomedical Sciences, University of California Riverside School of Medicine, Riverside, California, USA

[8]Neuroscience Center, University of Helsinki, Helsinki, Finland

[9]British Columbia Children's Hospital Research Institute, Department of Medical Genetics, University of British Columbia, Vancouver, British Columbia, Canada

Correspondence
Maija L. Castrén, Department of Physiology, Faculty of Medicine, University of Helsinki, P.O. Box 63, FI-00290 Helsinki, Finland.
Email: maija.castren@helsinki.fi

Funding information
Arvo and Lea Ylppö Foundation; Finnish Concordia Fund; FRAXA Research Foundation; Lastentautien Tutkimussäätiö; Michael Smith Foundation for Health Research; Suomen Akatemia; The Finnish Cultural Foundation; The Finnnish Brain Foundation

Abstract

The function of astrocytes intertwines with the extracellular matrix, whose neuron and glial cell-derived components shape neuronal plasticity. Astrocyte abnormalities have been reported in the brain of the mouse model for fragile X syndrome (FXS), the most common cause of inherited intellectual disability, and a monogenic cause of autism spectrum disorder. We compared human FXS and control astrocytes generated from human induced pluripotent stem cells and we found increased expression of urokinase plasminogen activator (uPA), which modulates degradation of extracellular matrix. Several pathways associated with uPA and its receptor function were activated in FXS astrocytes. Levels of uPA were also increased in conditioned medium collected from FXS hiPSC-derived astrocyte cultures and correlated inversely with intracellular Ca^{2+} responses to activation of L-type voltage-gated calcium channels in human astrocytes. Increased uPA augmented neuronal phosphorylation of TrkB within the docking site for the phospholipase-Cγ1 (PLCγ1), indicating effects of uPA on neuronal plasticity. Gene expression changes during neuronal differentiation preceding astrogenesis likely contributed to properties of astrocytes with FXS-specific alterations that showed specificity by not affecting differentiation of adenosine triphosphate (ATP)-responsive astrocyte

Ulla-Kaisa Peteri and Juho Pitkonen contributed equally to this study.

population. To conclude, our studies identified uPA as an important regulator of astrocyte function and demonstrated that increased uPA in human FXS astrocytes modulated astrocytic responses and neuronal plasticity.

KEYWORDS
astrocyte, fragile X syndrome, neuronal plasticity, urokinase plasminogen activator

1 | INTRODUCTION

Astrocytes are important in neuronal maturation and synapse function via bidirectional astrocyte-neuron interactions (Durkee & Araque, 2019; Vasile et al., 2017; Verkhratsky et al., 2014). They provide trophic support to neurons and contribute to brain homeostasis by regulating the extracellular environment. Astrocytes monitor and modulate synaptic transmission by controlling extracellular ion and neurotransmitter concentration in response to cytoplasmic Ca^{2+} fluctuations (Südhof, 2018). Molecules produced and released from astrocytes and neurons form extracellular matrix structures, which play important role in cell migration, neurite outgrowth, synaptogenesis, and synaptic plasticity (Song & Dityatev, 2018).

Malfunction of astrocytes is associated with many brain disorders (Molofsky et al., 2012). Deficits of astrocytes are shown to contribute to impaired neuronal function in the brain of *Fmr1* knockout (KO) mice, a mouse model of fragile X syndrome (FXS) (Simhal et al., 2019). The syndrome is the most common cause of inherited intellectual disability and a well-characterized monogenic form of autism spectrum disorder (ASD), with a prevalence around one in 4000 males and one in 8000 females (Crawford et al., 1999). The FXS phenotype includes hyperactivity, attention deficits, sensory integration problems, communication difficulties, poor motor coordination, social anxiety, and stereotyped patterns of behavior (Lozano et al., 2016; Terraciano et al., 2005). Epilepsy manifests in around 20% of cases (Berry-Kravis, 2002; Louhivuori et al., 2009) and criteria for ASD are fulfilled in 30%–54% of FXS males (Hagerman et al., 2010). FXS results from the absence of the FMR1 protein (FMRP) caused by transcriptional silencing of the *FMR1* gene with the expansion mutation comprising >200 cytosine-guanine-guanine (CGG) trinucleotide repeats (Colak et al., 2014). FMRP is an RNA-binding protein that is essential for normal synapse growth and function (Jin & Warren, 2000).

Coculturing *Fmr1* KO neurons with wild type astrocytes rescues the abnormal dendritic phenotype (Jacobs & Doering, 2010), supporting the role for astrocytes in the pathophysiology of FXS. Selective absence of astroglial FMRP augments neuronal excitability, increases spine density in the motor cortex, and alters the mouse behavioral phenotype (Higashimori et al., 2013; Hodges et al., 2017). The plasminogen system is affected in the brain of *Fmr1* KO mouse appearing increased expression of tissue plasminogen activator (tPA) in neural progenitors and astroglia (Achuta et al., 2014). *Fmr1* KO astrocytes express less thrombospondin-1 (TSP-1) (Cheng et al., 2016) that is a matricellular protein, which can mediate synaptic recovery induced by urokinase-type plasminogen activator receptor (uPAR)-activated astrocytes (Diaz et al., 2017). Both uPAR and its ligand urokinase (uPA) are highly abundant in the developing central nervous system, and are activated in many disease states (Blasi & Carmeliet, 2002). Upon binding to uPAR, uPA catalyzes plasminogen activation, and plasmin generation as the initiation of the proteolysis cascade, but it also activates cell-signaling pathways involved in the regulation of differentiation, cellular adhesion, migration, and proliferation through non-plasminogenic mechanisms (Blasi & Carmeliet, 2002). Despite potential contribution of uPA/uPAR signaling to the extracellular matrix-linked pathophysiology in FXS (Wen et al., 2018), the signaling system has not been studied with respect to FMRP.

Patient-specific human induced pluripotent stem cells (hiPSC) that carry disease-specific information, differentiated toward the astrocyte lineage, provide an ideal human cell-based model to study disturbed molecular mechanisms in human astrocytes. The present study exploited hiPSC-derived astrocyte model to study alterations in human FXS astrocytes and revealed that uPA can act as a critical regulator of astrocyte function and astrocyte-neuron interactions in the absence of FMRP. The results demonstrate that uPA-linked astrocytic properties may contribute to patient-specific differences and prove useful when designing pharmacological interventions for neurodevelopmental disorders.

2 | MATERIALS AND METHODS

2.1 | Generation of human astrocytes

Human astrocytes were differentiated from single clones of hiPSC lines derived from FXS males (HEL69.6, HEL70.3, HEL70.6, and HEL100.2) and healthy male donors (HEL23.3, HEL24.3, HEL46.11, PO2/UEF-3A, and PO4/UEF-3B) characterized previously (Achuta et al., 2017; Achuta et al., 2018; Asikainen et al., 2015; Holmqvist et al., 2016; Trokovic et al., 2015). To avoid effects of genetic background, astrocytes were also differentiated from isogenic human embryonic stem cell (hESC) lines (Utami et al., 2020): control (H1) and *FMR1*KO carrying a fragile X mutation that was generated by CRISPR/Cas9 gene editing targeting exon 3 in the *FMR1* gene. The research using human cells was approved by the Ethics Committee of the Hospital District of Helsinki and Uusimaa. All the human cell lines used in the study are listed in Table 1.

Human pluripotent stem cells (hPSCs) were maintained on Matrigel-coated plates in Essential 8 medium (E8; Thermo Fisher Scientific Ltd., Vantaa, Finland). Astrocytes were differentiated as

TABLE 1 hPSC lines used in the study

hiPSC lines; normal	hiPSC lines; FXS	ESC lines
HEL23.3	HEL69.6	H1
HEL24.3	HEL70.3	*FMR1*KO
HEL46.11	HEL70.6	
PO2/UEF-3A	HEL100.2	
PO4/UEF-3B		
Asikainen et al. (2015), Trokovic et al. (2015), and Holmqvist et al. (2016)	Achuta et al., 2017, 2018	Utami et al., 2020

Abbreviations: FXS, fragile X syndrome; hiPSC, human induced pluripotent stem cells; hPSC, human pluripotent stem cell.

previously described (Peteri et al., 2020). Briefly, for differentiation, 80% confluent hPSCs were dissociated with 0.5 mM ethylenediaminetetraacetic acid (EDTA; Invitrogen, Carlsbad, CA) and plated on low-attachment 6-well plate in E8 with 20 ng/ml human basic fibroblast growth factor (bFGF2; Peprotech, Somerset County, NJ) and 20 μM Rho kinase inhibitor (Sigma-Aldrich, St. Louis, MO). On the following day, medium was changed to neuronal induction medium (Advanced DMEM/F12, 1X N2, 2 mM L-glutamine, 1X nonessential amino acids [NEAA], and 1X penicillin–streptomycin [P–S] [all from Thermo Fisher Scientific]) supplemented with 0.1 μM LDN-193189 (Stemgent), 1 μM cyclopamine (Sigma-Aldrich), 10 μM SB-431542 (Sigma-Aldrich), and 0.5 μg/ml DKK1 (Dickkopf-related protein 1; Peprotech) for culturing the first 12 days. Thereafter, neural progenitors were cultured in neuronal induction medium supplemented with 20 ng/ml brain-derived neurotrophic factor (BDNF; Peprotech) until day 30 (D30) and in neurosphere medium (Advanced DMEM/F12, 1X B27 -RA, 1X L-glutamate, 1X NEAA, 1X P–S [all from Thermo Fisher Scientific]) supplemented with 20 ng/ml bFGF2 and 20 ng/ml epidermal growth factor (Peprotech) until D60. Growth factors were added three times a week and spheres were dissociated approximately once per week manually.

At D60, spheres were dissociated and progenitors plated on poly-ornithine/laminin-coated (Sigma-Aldrich) culture plates in neurosphere medium supplemented with 20 ng/ml ciliary neurotrophic factor (Peprotech). Cells were passaged with Trypsin–EDTA (0.05%) (Thermo Fisher Scientific) approximately once per week and seeded at 20,000 cells/cm^2. After D75, cells had acquired astrocyte morphology and they were maintained on Matrigel-coated culture plates.

2.2 | Immucytochemistry

For the astrocyte marker analysis, cells were plated on ViewPlate-96 (PerkinElmer) with 5000 cells/well. Two days later, cells were fixed with 4% paraformaldehyde for 15 min at room temperature (RT) and washed three times with phosphate buffered saline (PBS). Before incubation with primary antibody overnight at 4°C and with secondary antibody for 1 h at RT, cells were blocked with 10% normal goat serum and 0.05% Triton X-100 in PBS for 1 h. Primary antibodies were chicken anti-GFAP (Abcam, ab#4674, 1:1000), rabbit anti-SOX9 (Cell Signaling, #82630, 1:400), rabbit anti-NF1A (Active Motif, #39397, 1:500), mouse anti-S100β (Sigma-Aldrich, #S-2532, 1:500), and mouse anti-MAP2 (Sigma, #M4403, 1:2500). Secondary antibodies were Alexa Fluor 488 goat anti-chicken, Alexa Fluor 546 goat anti-rabbit, and Alexa Fluor 635 goat anti-mouse (1:500, Invitrogen). Nuclei were stained with 4′6-diamino-2-phenylindole (DAPI; Sigma, D9542, 1:10000). The cells were imaged with Thermo Scientific CellInsight instrument and analyzed using ImageJ and CellProfiler software.

2.3 | RNA sequencing analysis

RNA sequencing (RNA-seq) data were generated using triplicate samples of isogenic hPSC (H1 and *FMR1*KO cell lines)-derived cells at defined time points during astrocyte differentiation and NextSeq500 platform. The sequencing reads were filtered based on quality and length, and after adapter removal the reads were aligned to the human genome using Star Aligner (version 2.5.0b) and counted with high-throughput sequencing. We sequenced 20–30 millions reads per sample and aligned them using STAR v2.7.0 that uniquely mapped 80%–90% of the reads on the GRCh38 human genome, after quality trimming of 25 nucleotides from the 3′-ends of the transcripts (discarding reads shorter than 30 nucleotides) using cutadapt v1.8.1. Differential expression analysis was performed with the R package DESeq2 using a design formula that models the cell line difference at time 0, the difference over time, and any genotype-specific difference over time (by using the interaction term genotype: time). The likelihood ratio test removed any genotype-specific differences over time. Principal component analysis (PCA) showed six outliers (one replicate of undifferentiated cells, two at D30, and one at D95 of controls, and one iPSC FXS sample), which were removed from the analysis. Part of the genotype effect was visible on Component 2. The relative expression levels of control and FXS hPSC-derived cells at D12, D30, and D60 of differentiation to undifferentiated cells at D0 were compared and subjected to functional enrichment analysis performed with gost function from the gprofiler2 R package (Raudvere et al., 2019). Visualization of the gprofiler GO enrichment results was performed with the rrvgo package (Sayols, 2020). In addition, comparison of the three D95 FXS samples to the two isogenic control samples was performed to detect genes whose final expression significantly differed. Follow-up analyses were performed with the clusterProfiler R package and included pathway enrichment analysis using the REACTOME database (Jassal et al., 2020) to assess significance by hypergeometric test and gene set enrichment analysis (GSEA) ranking genes by their statistics and using gene permutation of the ranked list for calculating the *p*-value of the enrichment scores.

2.4 | RNA extraction and RT-PCR

Total cellular RNA was extracted using NucleoSpin RNA kit (QIAGEN) according to the manufacturer's instructions and reverse-transcribed into complementary cDNA using iScriptTM cDNA synthesis kit (Bio-Rad, #170-8891). Using cDNA as template, RT-quantitative polymerase chain reaction (qPCR) was performed with HOT FIREPol® EvaGreen® qPCR Mix Plus (Solis BioDyne) and LightCycler® 480 (Roche) for 45 cycles of 95°C for 15 s, 62°C for 20 s, and 72°C for 20 s. Gene expressions were analyzed with the ΔΔCt method using GAPDH expression and values from undifferentiated hiPSCs for normalization. Glyceraldehyde 3-phosphate dehydrogenase (GAPDH) expression was not affected by the absence of FMRP in transcriptome analysis of astrocytes (data not shown). Primer sequences are listed in Table 2.

2.5 | Astrocyte conditioned medium

For collection of astrocyte conditioned medium (ACM) cells were plated on Matrigel-coated T25 flasks at a density of 20,000 cells/cm^2 and grown for 7 days. On the day prior to the sample collection, medium was replaced with 5 ml of fresh neurosphere medium. As indicated cells were treated with all-trans retinoic acid (ATRA) for 24 h. Collected medium was filtered through a 0.22 μm filter and stored at −80°C until use.

2.6 | Analysis of plasminogen activators in ACM

The quantitative measurements of uPA and tPA in ACM were performed according to the manufacturer's instructions using Abcam's Enzyme-Linked Immunosorbent Assay (ELISA, Abcam) for human uPA (ab119611) and tPA (ab190812). The concentrations in diluted (1:1) culture medium were measured in duplicate, interpolated from the standard curve, and corrected for sample dilution.

2.7 | Protein isolation and Western blot analysis

Cells were isolated, suspended in ×1 RIPA lyses buffer (Upstate) supplemented with 1% protease inhibitor cocktail (Sigma), triturated, and centrifuged at ×10,000 g for 10 min at 4°C. Total protein (40 μg) was separated on SDS-polyacrylamide gel electrophoresis, transferred to a nitrocellulose membrane using Trans-Blot Turbo System (BioRad) and probed with rabbit polyclonal anti-FMRP antibody (1:500, ab17722; Abcam) at 4°C overnight after blocking with 5% nonfat dry milk in PBS at RT for 1 h. After washes, incubation with horseradish-peroxidase conjugated secondary antibody (1:10000, NA9340; GE Healthcare) was performed and immunoreactive protein was visualized using Pierce enhanced chemiluminescence (ECL) substrate (Thermo Fisher Scientific).

2.8 | Calcium imaging

For calcium imaging, astrocytes were plated on coverslips in a 12-well plate with 50,000 cells per well and imaging was performed on the following day as previously described (Achuta et al., 2018). Cells were loaded with 4 μM Fura-2 (HelloBio, HB0780) in Hepes-buffered medium (pH 7.4) containing 137 mM NaCl, 5 mM KCl, 0.44 KH_2PO_4, 4.2 mM $NaHCO_3$, 1 mM $MgCl_2$, 1 mM $CaCl_2$, and 10 mM glucose (all from Sigma-Aldrich) at 37°C for 30 min. The coverslip was then adjusted to SA-OLY/20 adapter and placed in the recording chamber with continuous perfusion with 37°C Hepes-buffered medium (2 ml/min). Cells were excited with 340 and 380 nm wavelengths and the emission was recorded at 505 nm. Cell somas were outlined as regions of interests (ROIs), and $[Ca^{2+}]_i$ rise in each ROI was recorded. When recording high KCl-induced depolarization, NaCl was iso-osmotically replaced with 17 or 70 mM KCl. Anti-uPA antibody (1:2000, #119611, Abcam) and Nifedipine (10 μM, Sigma) were added as indicated. Using an Inverted IX70 microscope (Olympus Corporation, Hamburg, Germany) cells were visualized with (UApo/340) x10 air objective (Olympus) and images acquired with a Hamamatsu ORCA-Flash 4.0 camera. An image (ratio 340 nm/380 nm) was acquired each second and up to 100 cells were recorded simultaneously. Data analysis was performed using HCImage and Matlab.

2.9 | Analysis of TrkB phosphorylation

Primary cultures of cortical neurons were prepared from E18 rat embryos as described previously (Sahu et al., 2019). Cells were maintained in supplemented NeuroBasal medium until D8 in vitro and incubated with pooled ACM from hiPSC-derived astrocytes supplemented with anti-uPA antibody (1:2000, #119611, Abcam) or TrkB.Fc (200 ng/ml; 688-TK, R&D Systems, Minneapolis, MN) as indicated for 30 min and lysed in neural progenitor lysis buffer (20 mM Tris–HCl; 137 mM NaCl; 10% glycerol; 50 mM NaF; 1% NP-40; 0.05 mM Na_3VO_4; containing a cocktail of protease and phosphatase inhibitors [#P2714 and #P0044, respectively, Sigma-Aldrich]). As a control test, rat cortical neurons were treated with recombinant rat urokinase protein (5 ng/ml, #92608, Abcam) for 1 h. The phosphorylation of different TrkB residues were determined by ELISA (Fred

TABLE 2 Primers used in qPCR analysis

Gene	Forward primer (5′-3′)	Reverse primer (5′-3′)
GAPDH	AACGACCCCTTCATTGAC	TCCACGACATACTCAGCAC
PLAU	GCCTTGCTGAAGATCCGTTC	GGATCGTTATACATCGAGGGGCA
PLAUR	CGGGCTCCAATGGTTTCCA	CAGAGTGAGCGTTCGTGAGTG
Serpine-1	CTTGCAATGGGAATGATGGAACTTG	CGAAATCATGTCCACTTGTGTTCAT

et al., 2019). Briefly, white 96-well plates (OptiPlate 96F-HB, Perkin Elmer) were coated with primary anti-TrkB antibody (1:1000, #AF1494, R&D Systems) in carbonate buffer (pH 9.8) overnight at 4°C. Following a blocking step with 3% BSA in PBST (137 mM NaCl, 10 mM phosphate, 2.7 mM KCl, 0.1% Tween-20; pH 7.4) for 2 h at RT, samples were incubated overnight at 4°C. The incubation with antibody against pTrkB^{Y816} (1:1000, #4168, Cell Signaling) or pTRKB^{Y515} (1:1000, #9141, Cell Signaling) was followed by the incubation with HRP (horseradish peroxidase)-conjugated anti-Rb (#170–5046, Bio-Rad) for 2 h at RT. Finally, the chemiluminescent signal generated by the reaction with ECL substrate was analyzed in a plate reader (Varioskan Flash, Thermo Fisher Scientific).

2.10 | Statistical analysis

Data are means ± SEM. Statistical comparisons were performed with two-tailed Student's unpaired *t* test, one-way ANOVA followed by post hoc Bonferroni test and Mann–Whitney test in analysis of $[Ca^{2+}]_i$, and two-way ANOVA and Fisher's LSD post hoc test in TrkB phosphorylation experiments using IBM SPSS analysis software. A *p*-value of <.05 was considered statistically significant.

3 | RESULTS

3.1 | Differentiation of astrocytes modeling FXS

We used hPSC-derived forebrain astrocyte model (hASTRO) meaning astrocytes at D95 of differentiation in vitro (Peteri et al., 2020) to study putative alterations of human FXS astrocytes (Figure 1a). Differentiation of astrocytes followed the developmental processes of astrocytes from neuroepithelial induction and regional patterning using morphogens to progenitor expansion and astrocyte specification/maturation (Russ et al., 2021). We monitored the differentiation of isogenic FXS and control hESC-derived cells by RNA-seq transcriptomic analysis at D0, D12, D30, D60, and D95 of differentiation (Figure 1a). PCA analysis of lineage-specific marker expression and hierarchical clustering showed that undifferentiated cells clearly separated from clusters of differentiated cells (Figure 1b). FMRP-deficient and their isogenic control cells clustered together at all-time points (Figure 1b). At D95, both FXS and control hASTRO clustered together with previously published human astrocytes isolated from the embryonic brain and hiPSC-derived astrocytes generated with an alternative differentiation protocol (Figure 1b) (Magistri et al., 2016; Tcw et al., 2017).

Immunostaining of hASTRO generated from the isogenic FXS and control cell lines and also from four patient-specific FXS and four control hiPSC lines demonstrated that over 90% of cells showed immunoreactivity for established astrocyte markers SOX9, NF1A, GFAP, and S100β (Figure 2a,b). Co-expression of GFAP and S100β was found in 98% of cells, suggesting that the hASTRO represented immature rather than mature astrocytes in the same way as the previously published hPSC-derived astrocytes (Tcw et al., 2017). Astrocyte marker

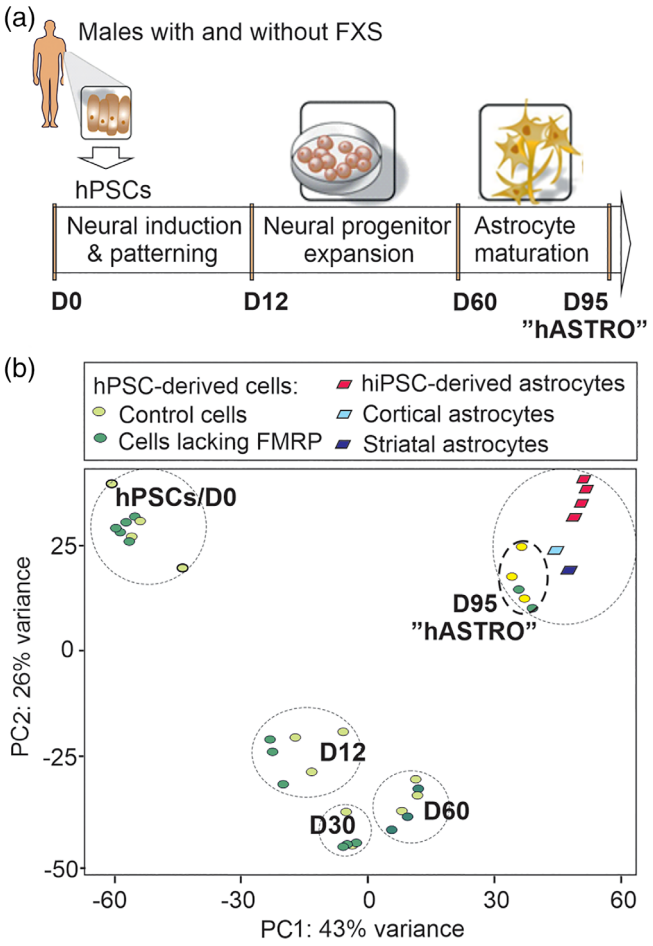

FIGURE 1 Differentiation of human pluripotent stem cell (hPSC)-derived astrocytes modeling fragile X syndrome (FXS). (a) Schematic representation of the astrocyte differentiation protocol to generate hASTRO. (b) Principal component analysis of lineage-specific marker expression in hPSC-derived cells carrying mutation causing FXS (green circles) and their isogenic controls (yellow circles) at Day 0 (D0), D12, D30, D60, and D95, showing clustering of D95 astrocytes (hASTRO) together with previously published astrocytes generated from hPSCs using alternative methods and with fetal astrocytes isolated from the midbrain and cortex

immunostaining of hASTRO suggested high purity of the astrocyte cultures. The number of MAP2 immunoreactive cells was less than 1% of total cells and the number of small MAP+ neuron-like cells did not differ between FXS and control hASTRO cultures (0.40 ± 0.42% in FXS and 0.48 ± 0.25% in control cultures) (Figure 2c). Western analysis confirmed that FXS hASTRO generated from both hiPSC lines with >200 CGG triplet repeats mutation in the *FMR1* gene and from *FMR1*KO hESCs did not express FMRP (Figure 2d).

3.2 | Transcriptome analysis of FXS cells during astrocyte differentiation

Factors that are closely linked to control of neurogenesis induce gliogenesis (Takouda et al., 2017). Transcriptome analysis of

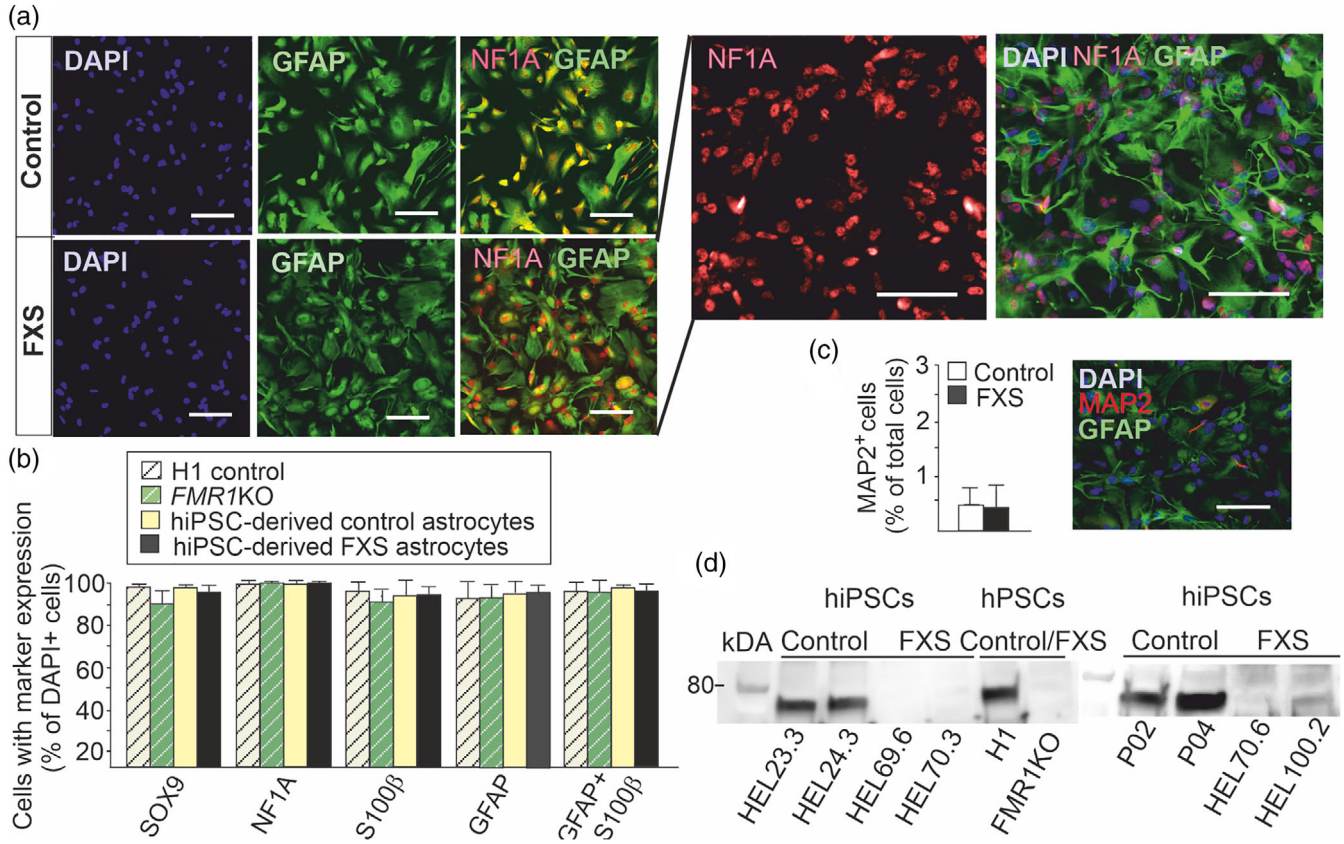

FIGURE 2 Characterization of human astrocyte model hASTRO. (a) Representative images of FXS and control hASTRO immunostained for GFAP (green) and NF1A (red). Staining of nuclei with DAPI, 4′,6′-diamidino-2-phenylindole (blue). Immunostaining for NF1A and an overlay of NF1, GFAP, and DAPI staining are shown enlarged. (b) Proportion of cells immunoreactive for astrocyte markers (SOX9, NF1A, S100β, and GFAP) in FXS hASTRO (*FMR1*KO and 3 FXS hiPSC lines) and controls (H1 isogenic control and three control hiPSC lines). (c) Proportion of cells immunoreactive for neuronal marker MAP2 in FXS and control hASTRO cultures ($n = 5$ in both experimental groups). Representative image of hASTRO immunostained for MAP2 (red), GFAP (green), and DAPI (blue). (d) Expression of FMRP in hASTRO derived from FXS and control cell lines used in the study. Data are means ± SEM. Scale bars 50 μm

differentiating isogenic neural progenitors lacking FMRP and their controls showed similar changes in the expression of factors that regulate the onset of gliogenesis and/or are known as early astrocyte markers (*SOX9*, *NF1A*, *SLIT-1*, *FGF3*, and *GLI3*) (Figure 3a). Transcriptome profiling also validated patterning of cells toward forebrain identity by increased expression of regional transcription factors (Rubenstein et al., 1998; Takouda et al., 2017) in both FXS and control cell cultures. Rostral genes *FOXG1*, *LHX2*, *EMX1*, and *DLX1* were expressed similarly in high levels, while the midbrain-associated genes *EN1*, *EN2*, and *FOXA2* and the hindbrain marker *HOXA2* were expressed at very low levels during the differentiation of isogenic neural progenitors derived from FXS and control cell lines (Figure 3b).

In agreement with the previous studies showing altered differentiation of neural progenitors lacking FMRP (Achuta et al., 2017; Achuta et al., 2018; Boland et al., 2017; Li & Zhao, 2014; Telias & Ben-Yosef, 2014; Utami et al., 2020), comparison of the transcriptome of FXS neural progenitors to controls at D12 showed differential expression of several genes; altogether 3276 genes were differentially regulated (Figure 3c). Transcripts of 433 and 2843 genes were increased and reduced, respectively, in D12 neurospheres. Many of these genes (~24%) remained differentially regulated at D30 (Figure 3c). Functional annotation analysis revealed that biological processes related to nervous system development, synaptic signaling, and axonogenesis were activated in FXS neural progenitors at D30 (Figure 3d). The absence of FMRP suppressed several biological processes, including immune response, positive regulation of cytosolic calcium ion responses and cytokine production, response to other organism, and defense response, and activity of cell surface signaling pathway (Figure 3e). These gene expression changes in neural progenitors likely influenced differentiation of astrocytes with FXS-specific properties in vitro and presumably have impact on neurogenesis and gliogenesis in the developing FXS brain.

Comparison of RNA seq data of hESC-derived isogenic FXS and control hASTRO at D95 revealed 81 differentially regulated transcripts (Table 3). Genes implicated in the extracellular matrix organization were particularly enriched among the differentially regulated genes (Figure 4a). A strong enrichment for genes involved in integrin cell surface interaction was found ($p = .045$, p adjusted $= .0174$, GSEA) in the gene ranking (Figure 4b). Enrichment of genes encoding proteins involved in the MET signaling cascade provided a potential

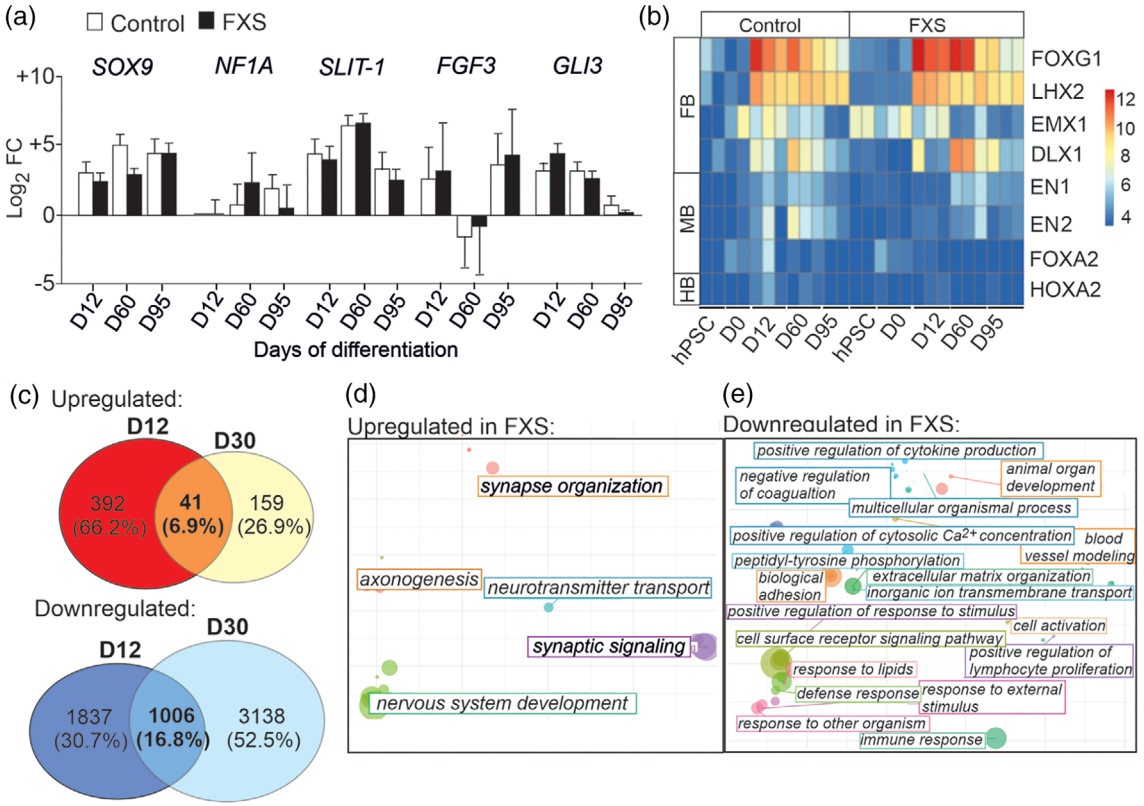

FIGURE 3 Glial fate determination and patterning of neural progenitors lacking FMRP. (a) Expression of *SOX9*, *NF1A*, *SLIT-1*, *FGF3*, and *GLI3* in the transcriptome analysis of cells differentiated from *FMR1*KO and its isogenic control H1 cell line at D12 ($n = 3$), D60 ($n = 3$), and D95 hASTRO ($n = 2$) relative to the expression at D0 during astrocyte differentiation. Error bars represent SD (b) Expression of the forebrain (FB) genes (*FOXG1*, *LHX2*, *EMX1*, and *DLX1*), the midbrain (MB)-associated genes (*EN1*, *EN2*, and *FOXA2*), and the hindbrain (HB) marker (*HOXA2*) in FXS and control cells during astrocyte differentiation. (c) The number of genes regulated differentially in the transcriptome of D12 and D30 FXS and control neural progenitors. The overlapping region of the circles shows the number of genes regulated similarly at these differentiation time points. (d, e) Scatter plots produced by rrvgo of enriched GO terms (biological process) identified with gprofiler. Distances between points represent the similarity between terms and the size the points is proportional to the enrichment score ($-\log_{10}$(adjusted p-value))

link to the pathophysiology of ASD. Genetic studies have associated the *MET* allele with ASD (Campbell et al., 2006) and MET signaling has been shown to be disrupted in ASD (Campbell et al., 2008). MET is a receptor tyrosine kinase that directly modulates WNT/β-catenin signaling (Kim et al., 2013) in line with the enrichment of transcripts of WNT signaling pathway ($p = .001$, p adjusted $= .0228$, GSEA) in FXS hASTRO genes (Figure 4c). These results were consistent with previous studies showing that the WNT/β-catenin signaling pathway is affected and involved in altered fate specification of neural progenitors in FXS (Casingal et al., 2020; Luo et al., 2010).

Transcripts of several enriched genes ($p = .0098$, p adjusted $= .0579$, GSEA) in the upregulated portion of the FXS hASTRO transcriptome were linked to the plasminogen system that is also associated with MET signaling (Figure 5a). The RNA seq data suggested dysregulated expression of genes encoding uPA (*PLAU*), receptor for uPA (*PLAUR*), and plasminogen activator inhibitor-1, PAI-1 (*SERPINE1*), during differentiation of FXS hASTRO when compared with controls (Figure 5a,b). PAI-1 is a member of serine protease inhibitor (serpin) family and the principal inhibitor of uPA and tPA (see review Sillen & Declerck, 2021). From *SERPINE2* and *SERPINE3* paralogs, *SERPINE2* was expressed in FXS and control hASTRO in the same way, while *SERPINE3* expression was not detectable in astrocytes as reported previously (Lindner et al., 1986).

3.3 | Increased uPA mRNA expression in FXS astrocytes

We used hASTRO differentiated from four FXS male-derived hiPSC lines and three control cell lines to study alterations of plasminogen system in human FXS astrocytes in detail. The expression of *PLAU* had increased 3-fold ($p = .003$) in hiPSC-derived FXS hASTRO compared with controls (Figure 5c). Expression of the gene encoding uPAR, *PLAUR*, was 1.2-fold higher in FXS hASTRO than in controls but the difference did not reach the level of significance ($p = .083$) (Figure 5c). The mRNA expression of *SERPINE1* showed high variation between biological samples, but the 5-fold reduction in the ratio of *PLAU* mRNA to *SERPINE1* mRNA in FXS hASTRO suggested a crucial role for PAI-1 in the regulation of uPA function (Figure 5d).

TABLE 3 The differentially regulated genes in the transcriptome analysis of isogenic FXS and control hASTRO

Id	Base mean	log2FoldChange	lfcSE	stat	pval	padj	Gebe symbol
ENSG00000187601	136.1	−7.2	0.7	−10.2	2.0E-24	3.1E-20	MAGEH1
ENSG00000129824	362.2	−12.2	1.3	−9.8	8.2E-23	6.1E-19	RPS4Y1
ENSG00000165169	125.7	−10.7	1.3	−8.6	1.2E-17	6.3E-14	DYNLT3
ENSG00000102349	98.8	−10.4	1.3	−7.9	2.0E-15	7.8E-12	KLF8
ENSG00000181218	82.7	−9.1	1.3	−7.2	4.6E-13	1.4E-09	H2AW
ENSG00000196890	40.6	−7.3	1.2	−6.2	4.9E-10	1.3E-06	H2BU1
ENSG00000144583	209.7	6.5	1.2	5.4	7.3E-08	0.0002	MARCHF4
ENSG00000174080	24.7	−7.4	1.5	−5.1	2.9E-07	0.0006	CTSF
ENSG00000154736	92.4	4.9	1.0	5.0	6.4E-07	0.001	ADAMTS5
ENSG00000166897	126.6	6.4	1.3	4.9	7.7E-07	0.001	ELFN2
ENSG00000020181	171.4	5.2	1.1	4.9	9.6E-07	0.001	ADGRA2
ENSG00000158560	85.9	6.6	1.4	4.9	1.1E-06	0.001	DYNC1I1
ENSG00000122367	94.3	6.0	1.3	4.5	6.5E-06	0.008	LDB3
ENSG00000251129	44.2	−3.2	0.7	−4.5	8.0E-06	0.009	LINC02506
ENSG00000117115	107.3	5.5	1.2	4.4	1.1E-05	0.011	PADI2
ENSG00000115414	56867.9	4.3	1.0	4.3	1.4E-05	0.012	FN1
ENSG00000171388	74.1	4.4	1.0	4.3	1.4E-05	0.012	APLN
ENSG00000175274	1435.2	3.8	0.9	4.4	1.4E-05	0.012	TP53I11
ENSG00000182752	367.6	3.8	0.9	4.3	1.5E-05	0.013	PAPPA
ENSG00000224559	15.2	7.1	1.7	4.3	1.9E-05	0.015	LINC01087
ENSG00000178860	79.7	8.0	1.9	4.2	2.4E-05	0.018	MSC
ENSG00000138759	452.3	3.7	0.9	4.0	5.8E-05	0.040	FRAS1
ENSG00000151572	270.6	3.1	0.8	4.0	5.8E-05	0.040	ANO4
ENSG00000167641	88.6	4.8	1.2	4.0	6.3E-05	0.041	PPP1R14A
ENSG00000101335	17841.0	2.2	0.6	4.0	7.4E-05	0.046	MYL9
ENSG00000101333	650.2	3.8	1.0	3.9	8.5E-05	0.050	PLCB4
ENSG00000108821	280379.8	3.5	1.0	3.9	8.7E-05	0.050	COL1A1
ENSG00000113319	558.6	2.8	0.7	3.9	0.0001	0.051	RASGRF2
ENSG00000149295	54.4	6.5	1.7	3.9	9.8E-05	0.051	DRD2
ENSG00000161638	802.5	3.8	1.0	3.9	0.0001	0.051	ITGA5
ENSG00000173546	676.0	3.8	1.0	3.9	9.3E-05	0.051	CSPG4
ENSG00000187955	2199.5	2.9	0.8	3.9	0.0001	0.051	COL14A1
ENSG00000111057	232.3	3.4	0.9	3.9	0.0001	0.054	KRT18
ENSG00000145936	284.8	3.7	1.0	3.9	0.0001	0.054	KCNMB1
ENSG00000204460	11.1	−4.8	1.3	−3.9	0.0001	0.054	LINC01854
ENSG00000166147	7398.4	3.3	0.9	3.8	0.0001	0.057	FBN1
ENSG00000165757	102.7	4.3	1.1	3.9	0.0001	0.057	JCAD
ENSG00000116183	142.2	4.1	1.1	3.8	0.0001	0.059	PAPPA2
ENSG00000107731	469.2	3.7	1.0	3.8	0.0002	0.062	UNC5B
ENSG00000111424	106.7	3.3	0.9	3.8	0.0002	0.062	VDR
ENSG00000133392	3525.0	7.2	1.9	3.8	0.0002	0.062	MYH11
ENSG00000135269	325.7	3.4	0.9	3.8	0.0002	0.062	TES
ENSG00000204389	222.0	−1.5	0.4	−3.8	0.0002	0.062	HSPA1A
ENSG00000062038	96.6	3.9	1.0	3.7	0.0002	0.063	CDH3
ENSG00000123329	103.9	3.5	0.9	3.7	0.0002	0.063	ARHGAP9
ENSG00000125726	100.6	4.0	1.1	3.7	0.0002	0.063	CD70

TABLE 3 (Continued)

Id	Base mean	log2FoldChange	lfcSE	stat	pval	padj	Gebe symbol
ENSG00000158258	1928.6	2.8	0.7	3.7	0.0002	0.063	CLSTN2
ENSG00000173334	93.2	2.9	0.8	3.7	0.0002	0.063	TRIB1
ENSG00000204434	19.4	6.0	1.6	3.7	0.0002	0.063	POTEKP
ENSG00000128284	20.1	4.0	1.1	3.7	0.0002	0.064	APOL3
ENSG00000267095	34.4	4.2	1.1	3.7	0.0002	0.064	
ENSG00000113739	1154.5	3.4	0.9	3.7	0.0002	0.066	STC2
ENSG00000145423	438.5	6.5	1.8	3.7	0.0002	0.066	SFRP2
ENSG00000153071	847.1	2.7	0.7	3.7	0.0002	0.067	DAB2
ENSG00000073849	37.5	3.1	0.8	3.7	0.0003	0.069	ST6GAL1
ENSG00000132429	35.6	6.9	1.9	3.7	0.0003	0.069	POPDC3
ENSG00000157613	2311.4	3.2	0.9	3.7	0.0006	0.069	CREB3L1
ENSG00000159251	537.6	6.5	1.8	3.7	0.0003	0.069	ACTC1
ENSG00000277734	35.7	5.9	1.6	3.7	0.0003	0.069	TRAC
ENSG00000144339	483.0	3.2	0.9	3.7	0.0003	0.070	TMEFF2
ENSG00000131844	475.2	−1.1	0.3	−3.6	0.0003	0.073	MCCC2
ENSG00000143369	442.3	3.5	1.0	3.6	0.0003	0.074	ECM1
ENSG00000166922	43.4	3.2	0.9	3.6	0.0003	0.074	SCG5
ENSG00000173376	56.2	5.5	1.5	3.6	0.0003	0.074	NDNF
ENSG00000173530	524.6	2.3	0.6	3.6	0.0003	0.074	TNFRSF10D
ENSG00000205426	200.6	6.8	1.9	3.6	0.0003	0.074	KRT81
ENSG00000099337	41.4	4.8	1.3	3.6	0.0003	0.075	KCNK6
ENSG00000156453	195.8	3.4	1.0	3.6	0.0003	0.079	PCDH1
ENSG00000257219	46.6	5.7	1.6	3.6	0.0003	0.079	LNCOG
ENSG00000105976	207.8	2.4	0.7	3.6	0.0004	0.084	MET
ENSG00000162618	114.2	3.1	0.9	3.5	0.0004	0.089	ADGRL4
ENSG00000115232	691.6	3.3	0.9	3.5	0.0005	0.096	ITGA4
ENSG00000116329	36.8	5.3	1.5	3.5	0.0005	0.096	OPRD1
ENSG00000119699	1675.8	2.7	0.8	3.5	0.0005	0.096	TGFB3
ENSG00000123146	94.6	3.5	1.0	3.5	0.0005	0.096	ADGRE5
ENSG00000145934	6817.4	2.9	0.8	3.5	0.0005	0.096	TENM2
ENSG00000182247	209.6	1.9	0.6	3.5	0.0005	0.096	UBE2E2
ENSG00000198842	17.8	7.3	2.1	3.5	0.0005	0.096	DUSP27
ENSG00000203721	36.0	4.9	1.4	3.5	0.0005	0.096	LINC00862
ENSG00000130635	8600.7	2.6	0.8	3.5	0.0005	0.10	COL5A1
ENSG00000261150	569.2	1.8	0.5	3.5	0.0005	0.10	EPPK1

3.4 | Increase in extracellular uPA in FXS astrocyte cultures

To examine secretion of uPA from human astrocytes, we assessed uPA protein levels in ACM collected from control and FXS hASTRO cultures. We found that uPA was increased 5.5-fold ($p = .018$) in ACM of FXS hASTRO (Figure 5e), suggesting that FXS hASTRO secreted more uPA. As a control, we treated astrocytes with retinoic acid that increases uPA expression (Suzuki et al., 1999); treatment of hASTRO with ATRA increased uPA protein in both FXS and control ACM (Figure 5e). Since our previous studies have shown increased expression of tPA in neural progenitors and brain of *Fmr1* KO mice (Achuta et al., 2014), we also measured extracellular levels of tPA that differs in structure from uPA but mediates similar plasminogenic and non-plasminogenic effects in the brain. Levels of tPA were almost undetectable in ACM (less than 300 pg/ml) and tPA amounts did not differ in FXS and control samples (data not shown).

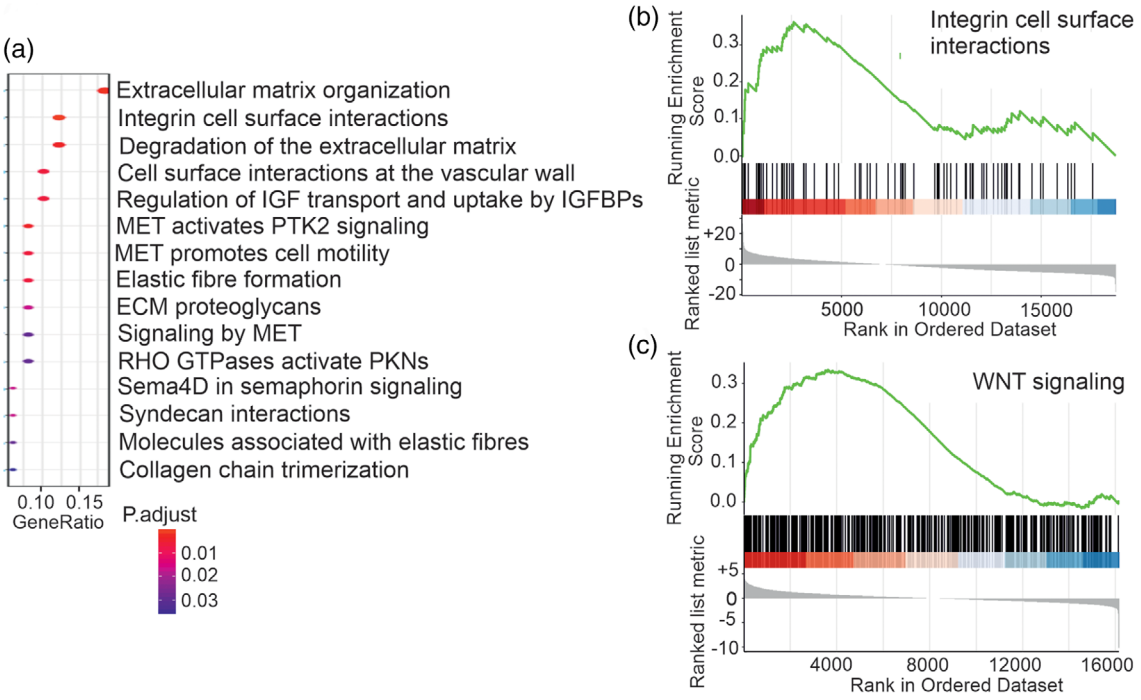

FIGURE 4 Functional annotation of RNA sequencing data of FXS and control astrocytes. (a) Pathway enrichment analysis of differentially expressed genes in FMRP-deficient and isogenic control ESC-derived D95 hASTRO using the REACTOME database. (b) Gene set enrichment analysis showing a significant positive enrichment score for the integrin cell surface interactions REACTOME pathway and (c) for the gene ontology WNT signaling pathway

3.5 | Extracellular uPA levels correlate with intracellular Ca^{2+} responses in hASTRO

To assess effects of increased uPA on astrocyte function, we studied intracellular Ca^{2+} ($[Ca^{2+}]_i$) responses of FXS hASTRO using Fura-2-based ratiometric Ca^{2+} measurements. As shown previously (Cheli et al., 2016), elevated external potassium (17 and 70 mM $[K^+]_e$) induced plasma membrane depolarization and Ca^{2+} influx via voltage-gated calcium channels (VGCCs) seen as a transient increase that was followed by a slow decline of $[Ca^{2+}]_i$ concentrations (Figure 6a). The transient $[Ca^{2+}]_i$ responses of cells in hASTRO cultures were relatively uniform in shape and size, suggesting high purity of astrocyte cultures. The specific L-type VGCC inhibitor nifedipine blocked the response (Figure 6a), indicating that the rise in $[Ca^{2+}]_i$ was caused by Ca^{2+} influx via L-type VGCCs.

In FXS hASTRO, the average amplitude of $[Ca^{2+}]_i$ responses to elevated $[K^+]_e$ was smaller (79% of controls; $p < .001$) than that in control hASTRO (Figure 6b). Also the proportion of cells showing $[Ca^{2+}]_i$ response was reduced (42% of controls; $p = .034$) in FXS hASTRO (Figure 6c). We found a strong correlation between the uPA amount in ACM and the proportion of cells responding to elevated $[K^+]_e$ ($R^2 = 0.786$, $p = .003$) (Figure 6d). Data obtained from altogether seven hiPSC lines showed that the higher the level of uPA was in ACM, the smaller the proportion of cells responsive to stimulation. An increase in $[Ca^{2+}]_i$ response to elevated $[K^+]_e$ after treatment with uPA antibody supported correlation between uPA/uPAR and L-type VGCC-mediated astrocytic calcium signaling (Figure 6e). The proportion of cells with $[Ca^{2+}]_i$ response to ATP (100 μM) and the average amplitude of ATP responses did not differ in FXS and control hASTRO (Figure 6f), supporting specificity of altered responses to elevated $[K^+]_e$ in FXS cells. Our results demonstrating that an increase in uPA/uPAR signaling in FXS hASTRO associated with reduced functional responses to elevated $[K^+]_e$ suggested a critical role for uPA in control of astrocyte function in FXS.

3.6 | Increased extracellular urokinase modulates neuronal plasticity

To elucidate consequences of increased uPA expression in FXS hASTRO, we investigated potential modulatory effects of increased extracellular uPA on neuronal function and thereby possible pro-maturational effects upon developing networks. Previous studies have shown that binding of neuronal uPA to astrocytic uPAR can activate astrocytes and promote neurological recovery after a hypoxic insult in vivo (Yepes, 2020). To test the neuronal effects of extracellular uPA, we exposed cultured rat primary cortical neurons to ACM collected from FXS and control hASTRO cultures and assessed the phosphorylation of TrkB neurotrophin receptors using ELISA. FXS ACM increased the phosphorylation of the phospholipase-Cγ1 (PLCγ1)-binding tyrosine within the TrkB ($TrkB^{Y816}$) (interaction: $F(2.90) = 7.318$, $p = .0011$; Figure 7a), but left the Shc binding site ($TrkB^{Y515}$) unaffected ($F(2.90) = 0.3119$, $p = .7328$; Figure 7b) in neurons when compared with the effects of control ACM. Treatment with uPA antibody prevented the increase in $TrkB^{Y816}$ phosphorylation,

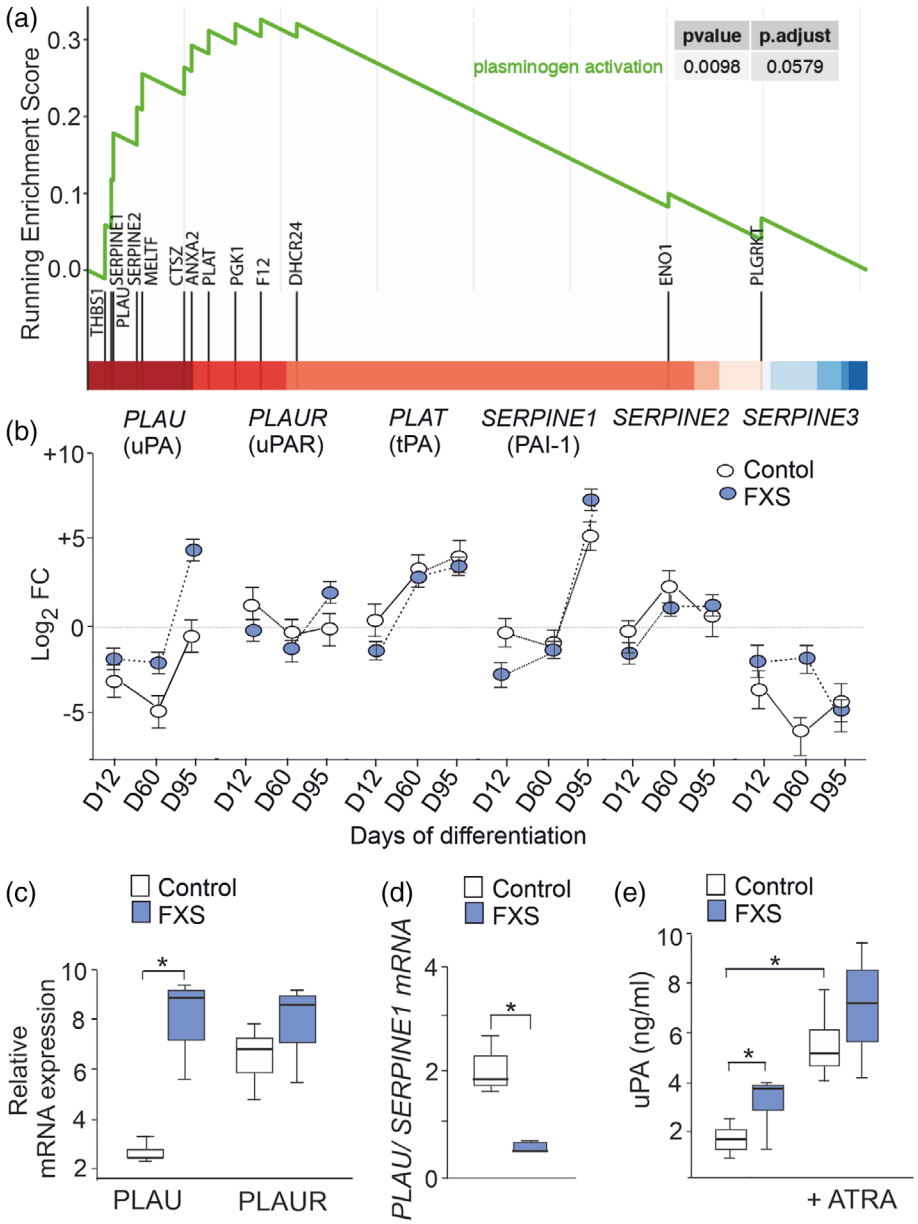

FIGURE 5 Increased expression of uPA in FXS compared with controls. (a) Gene set enrichment analysis revealed increased expression of genes encoding proteins involved in plasminogen system in FXS hASTRO compared with isogenic control at D95. (b) Expression of *PLAU*, *PLAUR*, *PLAT*, *SERPINE1*, *SERPINE2*, and *SERPINE3* in the transcriptome data of FXS and control isogenic cells at D12 ($n = 3$), D60 ($n = 3$), and D95 hASTRO ($n = 2$) relative to D0 during astrocyte differentiation. Abbreviation of the encoded protein is shown in parentheses. (c) Expression of *PLAU* and *PLAUR* mRNA and (d) the ratio of *PLAU* to *PLAUR* mRNA expression in D95 hASTRO generated from FXS hiPSCs compared with appropriate controls ($N = 3$ FXS and 3 control cell lines). (e) Abundance of uPA protein in astrocyte conditioned medium (ACM) collected from control and FXS hASTRO under basal conditions and after treatment with all-trans retinoic acid (ATRA) treatment ($N = 4$ FXS and 3 control cell lines). Data in boxplots show the median, the first and third quartiles, and the maximum and minimum values. Student's *t* test, $^{*}p < 0.05$

indicating that neuronal effects were mediated through uPA/uPAR signaling. Indeed, treatment with recombinant rat uPA (5 ng/ml) at the concentration range of FXS hASTRO medium increased the phosphorylation of $TrkB^{Y816}$ ($F(1.44) = 33.98$, $p < .0001$; Figure 7c). Treatment with antibody against TrkB ligand binding domain (TrkB.Fc) did not normalize the increase in neuronal TrkB phosphorylation (Figure 7a), suggesting that uPA enhanced responsiveness of TrkB receptors. Our results showing uPA/uPAR-mediated neuronal effects are in agreement with previous studies that have found stimulation of neuronal migration and axon growth by uPA/uPAR signaling (Yepes, 2020).

4 | DISCUSSION

Comparison of human astrocytes derived from FXS and control hiPSCs revealed increased expression of uPA in FXS astrocytes and their secretome, which associated with altered astrocytic gene expression linked to uPA/uPAR signaling and reduced $[Ca^{2+}]_i$ responses via L-type VGCCs. The data suggested that uPA-mediated effects were critical for astrocyte responsiveness. Furthermore, increased uPA in ACM collected from FXS astrocyte cultures augmented phosphorylation of TrkB within the PLCγ1 site in cortical neurons, indicating a role for uPA/uPAR signaling in the regulation of neuronal plasticity. The results demonstrated that uPA is an important regulator of astrocyte-neuron interactions, and that in the absence of FMRP altered uPA/uPAR signaling can modify properties of astrocytes and neuronal function. Previous studies provide evidence of cell type-specific changes, including abnormalities of BDNF/TrkB signaling and calcium dynamics, during differentiation of FMRP-deficient progenitors (Achuta et al., 2018; Achuta et al., 2017; Boland et al., 2017; Louhivuori et al., 2011; Telias et al., 2015; Utami et al., 2020). The uPA-mediated astrocytic mechanisms could serve as critical regulatory

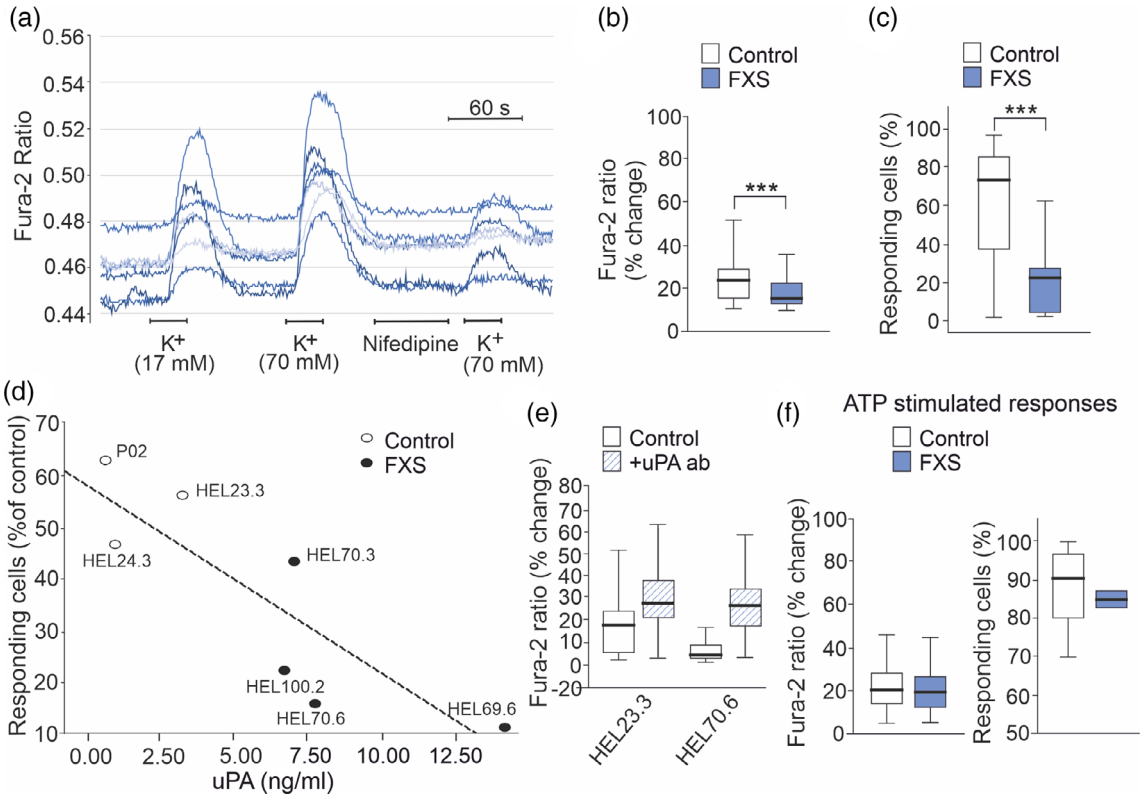

FIGURE 6 Intracellular calcium responses in human FXS and control hASTRO. (a) Representative cell responses in intracellular Ca^{2+} ($[Ca^{2+}]_i$) concentration after stimulation with high (17 and 70 μM) extracellular potassium ($[K^+]_e$) in hiPSC-derived D95 astrocytes (hASTRO). Nifedipine that is a specific inhibitor of L-type voltage-gated calcium channels blocked the response. Each trace corresponds to a single cell and the arrows indicate the time of high ($[K^+]_e$ and nifedipine (10 μM) addition. (b) The average amplitude of $[Ca^{2+}]_i$ responses, calculated from the responding cells expressed as a percentage of change of the emission intensities, and (c) the proportion of cells that showed $[Ca^{2+}]_i$ response to elevated $[K^+]_e$ in FXS and control hiPSC-derived hASTRO. $N = 4$ FXS and 4 controls. (d) Correlation of the amount of uPA in astrocyte conditioned medium and the number of cells responding to plasma membrane depolarization with elevated $[K^+]_e$ in control and FXS hASTRO. (e) Effects of uPA antibody treatment (1:2000) on the average amplitude of $[Ca^{2+}]_i$ responses to elevated $[K^+]_e$ in control (HEL23.3) and FXS (HEL70.6) hASTRO. (f) The average amplitude of $[Ca^{2+}]_i$ responses, calculated from the responding cells expressed as a percentage of change of the emission intensities, and the proportion of cells with $[Ca^{2+}]_i$ response to 100 μM ATP in FXS and control hiPSC-derived hASTRO. $N = 4$ FXS and 4 controls. Responses of 75–100 cells were measured in each experiment. Data are means ± SEM. Mann–Whitney–Wilcoxon test, $^{***}p < 0.001$

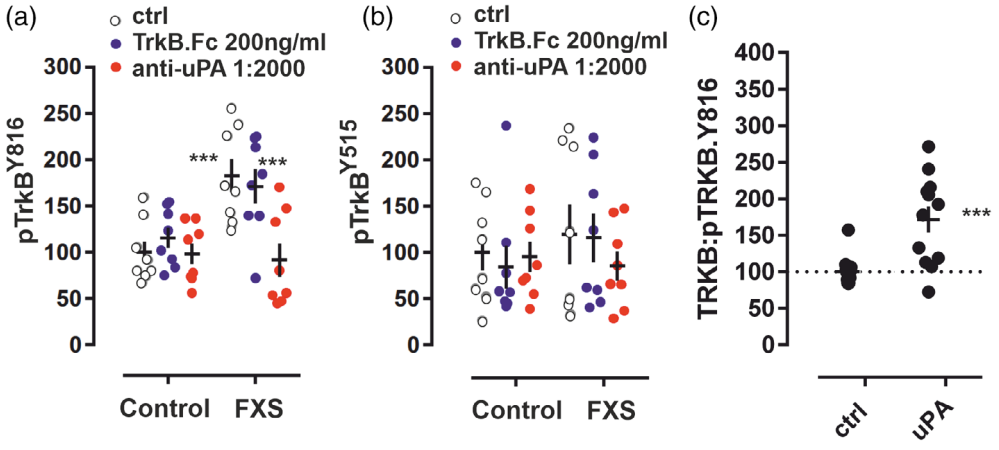

FIGURE 7 Effects of FXS astrocyte conditioned medium on TrkB receptor phosphorylation in neurons. Phosphorylation of (a) $TrkB^{Y816}$ and (b) $TrkB^{Y515}$ in primary rat cortical neurons treated with medium collected from FXS and control hiPSC-derived astrocyte cultures is shown under basal conditions (ctrl; white circles) and after treatment with antibody against ligand binding domain of TrkB (TrkB.Fc; blue) or with uPA antibody (red). $N = 4$ FXS and 3 control hiPSC cell lines. (c) Phosphorylation of $TrkB^{Y816}$ in primary rat cortical neurons treated with recombinant rat uPA. Data are means ± SEM. Two-way ANOVA and Fisher's LSD, $^{***}p < 0.001$

mechanisms maintaining cellular homeostasis that is compromised in the absence of FMRP, but they may also provide cellular feedback loop linked to neuronal BDNF/TrkB signaling (Louhivuori et al., 2011), which when dysregulated, could contribute to impaired neuronal plasticity and the phenotype of FXS.

The absence of FMRP altered the expression of several genes leading to FXS-specific changes during sequential differentiation of neural progenitors to functional astrocytes. However, the number of differentially expressed genes in FXS hASTRO at D95 of differentiation was limited to 81 genes when compared to controls. Abnormalities in the plasminogen system, especially related to uPA/uPAR emerged clearly in FXS hASTRO. Our data suggest that astrocytic uPA/uPAR signaling could provide an essential regulatory mechanism that convey messages from extracellular space to define functional properties of both astrocytes and neurons. Upon binding to its receptor, uPA catalyzes the conversion of plasminogen to plasmin on the cell surface, but uPAR also is able to engage in multiple protein/protein interactions (Blasi & Carmeliet, 2002). Since uPAR is devoid of a transmembrane and cytoplasmic domain, it needs a transmembrane partner to activate intracellular signaling. Integrins, G-protein receptors, and caveolin are mediators of uPA/uPAR signaling (Blasi & Carmeliet, 2002). We observed that increased uPA/uPAR signaling in FXS hASTRO associated with activated integrin function, consistent with coordinated actions of uPAR and integrins. The differentially regulated genes in FXS hASTRO included the *ADGRA2* gene encoding GPR124. This orphan receptor functions as a WNT7A/WNT7B-specific coactivator of canonical β-catenin signaling (Posokhova et al., 2015) and could potentially act as a transmembrane adaptor of uPAR and contribute to augmented activation of WNT signaling pathways observed in FXS hASTRO. WNT signaling regulates the differentiation of neural progenitors and the formation of neuronal circuits, playing roles in dendrite, and axon development (Oliva et al., 2018). Given that activation of WNT/β-catenin signaling can repress astrocyte specification (Sun et al., 2019), augmented WNT signaling together with reduced functional responses through L-type VGCCs in FXS hASTRO may indicate that lack FMRP affects specification astrocytes.

Both uPA and uPAR are developmentally regulated and their expression declines after peaking at the postnatal period to low or undetectable levels in the normal adult brain (Del Bigio et al., 1999). A transient increase of astrocytic uPAR is seen after cerebral ischemia (Yepes, 2020). In addition, involvement of the plasminogen system and uPA/uPAR signaling has been reported in brain tumors, multiple sclerosis, Alzheimer's disease, epilepsy, and developmental brain malformations (Akenami et al., 1997; Baart et al., 2020; Gveric et al., 2001; Iyer et al., 2010; Liu et al., 2010). Furthermore, a genetic link between the *PLAUR* gene and autism has been established integrated with MET signaling (Campbell et al., 2008). Involvement of uPAR in ASD was indicated by increased *PLAUR* mRNA expression in the postmortem ASD brain. The present study connected alterations of uPA/uPAR signaling with FXS, the most common genetic cause of ASD. The regulatory role of astrocytes in uPA/uPAR signaling and correlations of uPA levels with functional properties of astrocytes have not been previously described and our data provide novel insights to basic cellular mechanisms that could be disrupted in several forms of ASD. Impact of uPAR signaling in the developmental processes that define the adaptive capacity of cortical circuits was previously demonstrated in transgenic mice with genetic deletion of uPAR resulting in a reduced number of parvalbumin interneurons (Eagleson et al., 2010). Thus, uPA/uPAR signaling could contribute to synaptic excitation and inhibition balance that is affected in FXS and in many neurodevelopmental disorders (Gibson et al., 2008). Increased uPA/uPAR signaling in FXS hASTRO may reflect the abnormality and inability of astrocytes lacking FMRP to provide the normal neuronal support needed. Indeed, previous studies have demonstrated that coculturing of *Fmr1* KO mouse neurons with wild type mouse astrocytes shows rescue effects on the neuronal phenotype caused by FMRP deficiency (Jacobs & Doering, 2010).

Astrocytes comprise morphologically and functionally diverse populations of cells with brain region-specific differences in their properties. The differentiation method we employed produced homogenous cultures of human forebrain astrocytes expressing canonical astrocytic markers. The hASTRO were functional, as demonstrated by using intracellular calcium recordings, and allowed investigation of the innate properties of FXS astrocytes.

Astrocytes are crucial for synaptic and neuronal network formation and function, maintenance of brain homeostasis, and response to injury and repair. The astrocyte secretome illustrates astrocytic function. Rat primary cortical neurons were well suited for screening of the neuronal effects of FXS astrocyte secretome. Using a standardized method, murine primary neuronal cultures can be produced with minimal contribution of nonneuronal cells in a reliable and reproducible manner (Sahu et al., 2019). Since neurons do not divide in culture and they can be maintained for a limited period in culture, primary cortical, and hippocampal cultures need to be generated from embryonic or early postnal brain regions every time. Neuronal differentiation from stem cells, an unlimited source of progenitors, is current option that also allows generation of human neurons. Functional neurons can be differentiated from hiPSCs or fibroblast-direct conversion, but there are some variation in the differentiation efficiency depending on the used differentiation protocol. Effects of FXS hASTRO secretome remain to be validated in hiPSC-derived human neuronal cultures. Altered functional maturation of FXS hASTRO and effects of FXS hASTRO secretome on TrkB signaling in rat neurons suggested that astrocytes have a significant impact on neuronal network formation and function in FXS. Therefore, understanding of the special role of astrocytes in the FXS brain is important for the success of treatment strategies.

ACKNOWLEDGMENTS

We would like to thank the DNA Sequencing and Genomics Laboratory at the Institute of Biotechnology for the RNA sequencing analysis and Pia Laine together with Petri Auvinen for assisting with the data analysis. Imaging experiments were performed using services of the Biomedicum Imaging Unit. We also thank the Director of the Neuroscience Center Jari Koistinaho for the control hiPS cell lines. The work

was supported by the Academy of Finland, the Arvo and Lea Ylppö Foundation, the Finnish Konkordia Fund, the Finnish Cultural Foundation, the Finnish Brain Foundation, the Finnish Foundation for Pediatric Research, and the FRAXA Research Foundation. MAP is Michael Smith Foundation for Health Research Scholar.

AUTHOR CONTRIBUTION

Maija L. Castrén conceived the project and was responsible for project administration. Ulla-Kaisa Peteri generated astrocytes and performed most of the experiments. Laurent Roybon and Plinio Casorotto participated in the implementation of astrocyte differentiation and TrkB experiments, respectively. Tomas M. Strandin and Antti Vaheri helped with immunoassays. Juho Pitkonen analyzed data with assistance of Otso Nieminen. Ilario de Toma and Padraic Corcoran performed bioinformatics analyzes. Kagistia Hana Utami and Mahmoud A. Pouladi provided isogenic cell lines and contributed to the analysis of data. Maija L. Castrén wrote the manuscript. All authors have read and agreed to the published version of the manuscript.

CONFLICT OF INTEREST

The authors declare no potential conflict of interest.

DATA AVAILABILITY STATEMENT

The data that support the findings of this study are available from the corresponding author upon reasonable request.

ORCID

Juho Pitkonen https://orcid.org/0000-0002-4633-3578
Maija L. Castrén https://orcid.org/0000-0002-9644-5295

REFERENCES

Achuta, V. S., Möykkynen, T., Peteri, U.-K., Turconi, G., Rivera, C., Keinänen, K., & Castren, M. L. (2018). Functional changes of AMPA responses in human induced pluripotent stem cell-derived neural progenitors in autism spectrum disorder. *Science Signaling*, *11*, 1–11. https://doi.org/10.1126/scisignal.aan8784

Achuta, V. S., Putkonen, P., Grym, H., Louhivuori, V., Kärkkäinen, V., & Castrén, M. L. (2017). Metabotropic glutamate receptor 5 responses dictate differentiation of neural progenitors to NMDA-responsive cells in fragile X syndrome. *Developmental Neurobiology*, *4*, 438–453. https://doi.org/10.1002/dneu.22419

Achuta, V. S., Rezov, V., Uutela, M., Louhivuori, V., Louhivuori, L., & Castrén, M. L. (2014). Tissue plasminogen activator contributes to alterations of neuronal migration and activity-dependent responses in fragile X mice. *The Journal of Neuroscience*, *34*, 1916–1923. https://doi.org/10.1523/JNEUROSCI.3753-13.2014

Akenami, F. O. T., Koskiniemi, M., Mustjoki, S., Sirén, V., Färkkilä, M., & Vaheri, A. (1997). Plasma and cerebrospinal fluid activities of tissue plasminogen activator, urokinase and plasminogen activator inhibitor-1 in multiple sclerosis. *Fibrinolysis & Proteolysis*, *11*, 109–113. https://doi.org/10.1136/jcp.49.7.577

Asikainen, S., Heikkinen, L., Juhila, J., Holm, F., Weltner, J., Trokovic, R., Mikkola, M., Toivonen, S., Balboa, D., Lampela, R., Icay, K., Tuuri, T., Otonkoski, T., Wong, G., & Hovatta, O. (2015). Selective microRNA-offset RNA expression in human embryonic stem cells. *PLoS One*, *10*, e0116668. https://doi.org/10.1371/journal.pone.0116668

Baart, V. M., Houvast, R. D., de Geus-Oei, L. F., Quax, P. H. A., Kuppen, P. J. K., Vahrmeijer, A. L., & Sier, C. F. M. (2020). Molecular imaging of the urokinase plasminogen activator receptor: Opportunities beyond cancer. *EJNMMI Research*, *10*, 87. https://doi.org/10.1186/s13550-020-00673-7

Berry-Kravis, E. (2002). Epilepsy in fragile X syndrome. *Developmental Medicine and Child Neurology*, *44*, 724–728. https://doi.org/10.1017/s0012162201002833

Blasi, F., & Carmeliet, P. (2002). uPAR: A versatile signalling orchestrator. *Nature Reviews Molecular Cell Biology*, *3*, 932–943. https://doi.org/10.1038/nrm977

Boland, M. J., Nazor, K. L., Tran, H. T., Szücs, A., Lynch, C. L., Paredes, R., Tassone, F., Sanna, P. P., Hagerman, R. J., & Loring, J. F. (2017). Molecular analyses of neurogenic defects in a pluripotent stem cell model of fragile X syndrome. *Brain*, *40*, 582–598. https://doi.org/10.1093/brain/aww357

Campbell, D. B., Li, C., Sutcliffe, J. S., Persico, A. M., & Levitt, P. (2008). Genetic evidence implicating multiple genes in the MET receptor tyrosine kinase pathway in autism spectrum disorder. *Autism Research*, *1*, 159–168. https://doi.org/10.1002/aur.27

Campbell, D. B., Sutcliffe, J. S., Ebert, P. J., Militerni, R., Bravaccio, C., Trillo, S., Elia, M., Schneider, C., Melmed, R., Sacco, R., Persico, A. M., & Levitt, P. (2006). A genetic variant that disrupts MET transcription is associated with autism. *Proceedings of the National Academy of Sciences of the United States of America*, *103*, 16834–16839. https://doi.org/10.1073/pnas.0605296103

Casingal, C. R., Kikkawa, T., Inada, H., Sasaki, Y., & Osumi, N. (2020). Identification of FMRP target mRNAs in the developmental brain: FMRP might coordinate Ras/MAPK, Wnt/beta-catenin, and mTOR signaling during corticogenesis. *Molecular Brain*, *13*, 167. https://doi.org/10.1186/s13041-020-00706-1

Cheli, V. T., Santiago González, D. A., Smith, J., Spreuer, V., Murphy, G. G., & Paez, P. M. (2016). L-type voltage-operated calcium channels contribute to astrocyte activation in vitro. *Glia*, *64*, 1396–1415. https://doi.org/10.1002/glia.23013

Cheng, C., Lau, S. K. M., & Doering, L. C. (2016). Astrocyte-secreted thrombospondin-1 modulates synapse and spine defects in the fragile X mouse model. *Molecular Brain*, *9*, 74. https://doi.org/10.1186/s13041-016-0256-9

Colak, D., Zaninovic, N., Cohen, M. S., Rosenwaks, Z., Yang, W. Y., Gerhardt, J., Disney, M. D., & Jaffrey, S. R. (2014). Promoter-bound trinucleotide repeat mRNA drives epigenetic silencing in fragile X syndrome. *Science*, *343*, 1002–1005. https://doi.org/10.1126/science.1245831

Crawford, D. C., Meadows, K. L., Newman, J. L., Taft, L. F., Pettay, D. L., Gold, L. B., Hersey, S. J., Hinkle, E. F., Stanfield, M. L., Holmgreen, P., Yeargin-Allsopp, M., Boyle, C., & Sherman, S. L. (1999). Prevalence and phenotype consequence of FRAXA and FRAXE alleles in a large, ethnically diverse, special education-needs population. *American Journal of Human Genetics*, *64*, 495–507. https://doi.org/10.1086/302260

Del Bigio, M. R., Hosain, S., & Altumbabic, M. (1999). Localization of urokinase-type plasminogen activator, its receptor, and inhibitors in mouse forebrain during postnatal development. *International Journal of Developmental Neuroscience*, *17*, 387–399. https://doi.org/10.1016/s0736-5748(99)00031-3

Diaz, A., Merino, P., Manrique, L. G., Ospina, J. P., Wu, L. C. F., Jeanneret, V., & Yepes, M. (2017). A cross talk between neuronal urokinase-type plasminogen activator (uPA) and astrocytic uPA receptor (uPAR) promotes astrocytic activation and synaptic recovery in the ischemic brain. *The Journal of Neuroscience*, *37*, 10310–10322. https://doi.org/10.1523/JNEUROSCI.1630-17.2017

Durkee, C. A., & Araque, A. (2019). Diversity and specificity of astrocyte-neuron communication. *Neuroscience*, *396*, 73–78. https://doi.org/10.1016/j.neuroscience.2018.11.010

Eagleson, K. L., Gravielle, M. C., SchlueterMcFadyen-Ketchum, L. J., Russek, S. J., Farb, D. H., & Levitt, P. (2010). Genetic disruption of the autism spectrum disorder risk gene PLAUR induces GABAA receptor subunit changes. *Neuroscience*, *168*, 797–810. https://doi.org/10.1016/j.neuroscience.2010.03.066

Fred, S. M., Laukkanen, L., Brunello, C. A., Vesa, L., Göös, H., Cardon, I., Moliner, R., Maritzen, T., Varjosalo, M., Casarotto, P. C., & Castrén, E. (2019). Pharmacologically diverse antidepressants facilitate TRKB receptor activation by disrupting its interaction with the endocytic adaptor complex AP-2. *Journal of Biological Chemistry*, *294*, 18150–18161. https://doi.org/10.1074/jbc.RA119.008837

Gibson, J. R., Bartley, A. F., Hays, S. A., & Huber, K. M. (2008). Imbalance of neocortical excitation and inhibition and altered UP states reflect network hyperexcitability in the mouse model of fragile X syndrome. *Journal of Neurophysiology*, *100*, 2615–2626. https://doi.org/10.1152/jn.90752.2008

Gveric, D., Hanemaaijer, R., Newcombe, J., van Lent, N. A., Sier, C. F., & Cuzner, M. L. (2001). Plasminogen activators in multiple sclerosis lesions: Implications for the inflammatory response and axonal damage. *Brain*, *124*, 1978–1988. https://doi.org/10.1093/brain/124.10.1978

Hagerman, R., Hoem, G., & Hagerman, P. (2010). Fragile X and autism: Intertwined at the molecular level leading to targeted treatments. *Molecular Autism*, *1*, 1–14. https://doi.org/10.1186/2040-2392-1-12

Higashimori, H., Morel, L., Huth, J., Lindemann, L., Dulla, C., Taylor, A., Freeman, M., & Yang, Y. (2013). Astroglial FMRP-dependent translational down-regulation of mGluR5 underlies glutamate transporter GLT1 dysregulation in the fragile X mouse. *Human Molecular Genetics*, *22*, 2041–2054. https://doi.org/10.1093/hmg/ddt055

Hodges, J. L., Yu, X., Gilmore, A., Bennett, H., Tjia, M., Perna, J. F., Chen, C. C., Li, X., Lu, J., & Zuo, Y. (2017). Astrocytic contributions to synaptic and learning abnormalities in a mouse model of fragile X syndrome. *Biological Psychiatry*, *82*, 139–149. https://doi.org/10.1016/j.biopsych.2016.08.036

Holmqvist, S., Lehtonen, Š., Chumarina, M., Puttonen, K. A., Azevedo, C., Lebedeva, O., Ruponen, M., Oksanen, M., Djelloul, M., Collin, A., Goldwurm, S., Meyer, M., Lagarkova, M., Kiselev, S., Koistinaho, J., & Roybon, L. (2016). Creation of a library of induced pluripotent stem cells from Parkinsonian patients. *NPJ Parkinson's Disease*, *2*, 16009. https://doi.org/10.1038/npjparkd.2016.9

Iyer, A. M., Zurolo, E., Boer, K., Baayen, J. C., Giangaspero, F., Arcella, A., di Gennaro, G. C., Esposito, V., Spliet, W. G. M., van Rijen, P. C., Troost, D., Gorter, J. A., & Aronica, E. (2010). Tissue plasminogen activator and urokinase plasminogen activator in human epileptogenic pathologie. *Neuroscience*, *167*, 929–945. https://doi.org/10.1016/j.neuroscience.2010.02.047

Jacobs, S., & Doering, L. C. (2010). Astrocytes prevent abnormal neuronal development in the fragile X mouse. *The Journal of Neuroscience*, *30*, 4508–4514. https://doi.org/10.1523/JNEUROSCI.5027-09.2010

Jassal, B., Matthews, L., Viteri, G., Gong, C., Lorente, P., Fabregat, A., Sidiropoulos, K., Cook, J., Gillespie, M., Haw, R., Loney, F., May, B., Milacic, M., Rothfels, K., Sevilla, C., Shamovsky, V., Shorser, S., Varusai, T., Weiser, J., … D'Eustachio, P. (2020). The reactome pathway knowledgebase. *Nucleic Acids Research*, *48*, D498–D503. https://doi.org/10.1093/nar/gkx1132

Jin, P., & Warren, S. T. (2000). Understanding the molecular basis of fragile X syndrome. *Human Molecular Genetics*, *9*, 901–908. https://doi.org/10.1093/hmg/9.6.901

Kim, K. H., Seoul, H. J., Kim, E. H., Rheey, J., Jin, H. J., Lee, Y., Joo, K. M., Lee, J., & Nam, D. H. (2013). Wnt/β-catenin signaling is a key downstream mediator of MET signaling in glioblastoma stem cells. *Neuro-Oncology*, *15*, 161–171. https://doi.org/10.1093/neuonc/nos299

Li, Y., & Zhao, X. (2014). Concise review: Fragile X proteins in stem cell maintenance and differentiation. *Stem Cells*, *32*(7), 1724–1733. https://doi.org/10.1002/stem.1698

Lindner, J., Guenther, J., Nick, H., Zinser, G., Antonicek, H., Schachner, M., & Monard, D. (1986). Modulation of granule cell migration by a glia-derived protein. *Proceedings of the National Academy of Sciences of the United States of America*, *83*, 4568–4571. https://doi.org/10.1073/pnas.83.12.4568

Liu, B., Zhang, B., Wang, T., Liang, Q. C., Jing, X. R., Zheng, J., Wang, C., Meng, Q., Wang, L., Wang, W., Guo, H., You, Y., Zhang, H., & Gao, G. D. (2010). Increased expression of urokinase-type plasminogen activator receptor in the frontal cortex of patients with intractable frontal lobe epilepsy. *Journal of Neuroscience Research*, *88*, 2747–2754. https://doi.org/10.1002/jnr.22419

Louhivuori, V., Arvio, M., Soronen, P., Oksanen, V., Paunio, T., & Castrén, M. L. (2009). The Val66Met polymorphism in the BDNF gene is associated with epilepsy in fragile X syndrome. *Epilepsy Research*, *85*, 114–117. https://doi.org/10.1016/j.eplepsyres.2009.01.005

Louhivuori, V., Vicario, A., Uutela, M., Rantamäki, T., Louhivuori, L. M., Castrén, E., Tongiorgi, E., Åkerman, K. E., & Castrén, M. L. (2011). BDNF and TrkB in neuronal differentiation of Fmr1-knockout mouse. *Neurobiology of Disease*, *41*, 469–480. https://doi.org/10.1016/j.nbd.2010.10.018

Lozano, R., Azarang, A., Wilaisakditipakorn, T., & Hagerman, R. J. (2016). Fragile X syndrome: A review of clinical management. *Intractable and Rare Diseases Research*, *5*, 145–157. https://doi.org/10.5582/irdr.2016.01048

Luo, Y., Shan, G., Guo, W., Smrt, R. D., Johnson, E. B., Li, X., Pfeiffer, R. L., Szulwach, K. E., Duan, R., Barkho, B. Z., Li, W., Liu, C., Jin, P., & Zhao, X. (2010). Fragile X mental retardation protein regulates proliferation and differentiation of adult neural stem/progenitor cells. *PLoS Genetics*, *6*, e1000898. https://doi.org/10.1371/journal.pgen.1000898

Magistri, M., Khoury, N., Mazza, E. M. C., Velmeshev, D., Lee, J. K., Bicciato, S., Tsoulfas, P., & Faghihi, M. A. (2016). A comparative transcriptomic analysis of astrocytes differentiation from human neural progenitor cells. *The European Journal of Neuroscience*, *44*, 2858–2870. https://doi.org/10.1111/ejn.13382

Molofsky, A. V., Krenick, R., Ullian, E. M., Tsai, H., Deneen, B., Richardson, W. D., Barres, B. A., & Rowitch, D. H. (2012). Astrocytes and disease: A neurodevelopmental perspective. *Genes & Development*, *26*, 891–907. https://doi.org/10.1101/gad.188326.112

Oliva, C. A., Montecinos-Oliva, C., & Inestrosa, N. C. (2018). Wnt signaling in the central nervous system: New insights in health and disease. *Progress in Molecular Biology and Translational Science*, *153*, 81–130. https://doi.org/10.1016/bs.pmbts.2017.11.018

Peteri, U., Pitkonen, J., Utami, K. H., Paavola, J., Raybon, L., Pouladi, M., & Castrén, M. L. (2020). Generation of the human pluripotent stem-cell-derived astrocyte model with forebrain identity. *Brain Sciences*, *11*, 209. https://doi.org/10.3390/brainsci11020209

Posokhova, E., Shukla, A., Seaman, S., Volate, S., Hilton, M. B., Wu, B., Morris, H., Swing, D. A., Zhou, M., Zudaire, E., Rubin, J. S., & St Croix, B. (2015). GPR124 functions as a WNT7-specific coactivator of canonical β-catenin signaling. *Cell Reports*, *10*, 123–130. https://doi.org/10.1016/j.celrep.2014.12.020

Raudvere, U., Kolberg, L., Kuzmin, I., Arak, T., Adler, P., Peterson, H., & Vilo, J. (2019). G:Profiler: A web server for functional enrichment analysis and conversions of gene lists (2019 update). *Nucleic Acids Research*, *47*, W191–W198. https://doi.org/10.1093/nar/gkz369

Rubenstein, J. L., Shimamura, K., Martinez, S., & Puelles, L. (1998). Regionalization of the prosencephalic neural plate. *Annual Review of Neuroscience*, *21*, 445–477. https://doi.org/10.1146/annurev.neuro.21.1.445

Russ, K., Teku, G., Bousset, L., Redeker, V., Piel, S., Savchenko, E., Pomeshchik, Y., Savistchenko, J., Stummann, T. C., Azevedo, C., Collin, A., Goldwurm, S., Fog, K., Elmer, E., Vihinen, M., Melki, R., & Roybon, L. (2021). TNF-α and α-synuclein fibrils differently regulate human astrocyte immune reactivity and impair mitochondrial respiration. *Cell Reports*, *34*, 108895. https://doi.org/10.1016/j.celrep.2021.108895

Sahu, M. P., Nikkilä, O., Lågas, S., Kolehmainen, S., & Castrén, E. (2019). Culturing primary neurons from rat hippocampus and cortex. *Neuronal Signaling*, *3*, NS20180207. https://doi.org/10.1042/NS20180207

Sayols, S. (2020). Rrvgo: A bioconductor package to reduce and visualize gene ontology terms. https://ssayols.github.io/rrvgo

Sillen, M., & Declerck, P. J. (2021). A narrative review on plasminogen activator inhibitor-1 and its (patho)physiological role: To target or not to target? *International Journal of Molecular Sciences*, *22*, 2721. https://doi.org/10.3390/ijms22052721

Simhal, A. K., Zuo, Y., Perez, M. M., Madison, D. V., Sapiro, G., & Micheva, K. D. (2019). Multifaceted changes in synaptic composition and astrocytic involvement in a mouse model of fragile X syndrome. *Scientific Reports*, *9*, 13855. https://doi.org/10.1038/s41598-019-50240-x

Song, I., & Dityatev, A. (2018). Crosstalk between glia, extracellular matrix and neurons. *Brain Research Bulletin*, *136*, 101–108. https://doi.org/10.1016/j.brainresbull.2017.03.003

Südhof, T. (2018). Towards an understanding of synapse formation. *Neuron*, *100*, 276–293. https://doi.org/10.1016/j.neuron.2018.09.040

Sun, S., Xiao-Jing Zhu, X., Hao Huang, H., Wei Guo, W., Tao Tang, T., Xie, B., Xu, X., Zhang, Z., Shen, Y., Dai, Z.-M., & Qiu, M. (2019). WNT signaling represses astrogliogenesis via Ngn2-dependent direct suppression of astrocyte gene expression. *Glia*, *67*, 1333–1343. https://doi.org/10.1002/glia.23608

Suzuki, Y., Shimada, J., Shudo, K., Matsumura, M., Crippa, M. P., & Kojima, S. (1999). Physical interaction between retinoic acid receptor and Sp1: Mechanism for induction of urokinase by retinoic acid. *Blood*, *93*, 4264–4276.

Takouda, J., Katada, S., & Nakashima, K. (2017). Emerging mechanisms underlying astrogenesis in the developing mammalian brain. *Proceedings of the Japan Academy Series B: Physical and Biological Sciences*, *93*, 386–398. https://doi.org/10.2183/pjab.93.024

Tcw, J., Wang, M., Pimenova, A. A., Bowles, K. R., Hartley, B. J., Lacin, E., Machlovi, S. I., Abdelaal, R., Karch, C. M., Phatnani, H., Slesinger, P. A., Zhang, B., Goate, A. M., & Brennand, K. J. (2017). An efficient platform for astrocyte differentiation from human induced pluripotent stem cells. *Stem Cell Reports*, *9*, 600–614. https://doi.org/10.1016/j.stemcr.2017.06.018

Telias, M., & Ben-Yosef, D. (2014). Modeling neurodevelopmental disorders using human pluripotent stem cells. *Stem Cell Reviews*, *10*, 494–511. https://doi.org/10.1007/s12015-014-9507-2

Telias, M., Kuznitsov-Yanovsky, L., Segal, M., & Ben-Yosef, D. (2015). Functional deficiencies in fragile X neurons derived from human embryonic stem cells. *Journal of Neuroscience*, *35*, 15295–15306. https://doi.org/10.1523/JNEUROSCI.0317-15.2015

Terraciano, A., Chiurazza, P., & Neri, G. (2005). Fragile X syndrome. *American Journal of Medical Genetics. Part C, Seminars in Medical Genetics*, *137C*, 32–37. https://doi.org/10.1002/ajmg.c.30062

Trokovic, R., Weltner, J., & Otonkoski, T. (2015). Generation of iPSC line HEL24.3 from human neonatal foreskin fibroblasts. *Stem Cell Research*, *15*, 266–268. https://doi.org/10.1016/j.scr.2015.05.012

Utami, K. H., Skotte, N. H., Colaço, A. R., Yusof, N. A. B. M., Bernice Sim, B., Yeo, X. Y., Bae, H., Garcia-Miralles, M., Radulescu, C., Chen, Q., Chaldaiopoulou, G., Liany, H., Nama, S., Sampath, P., Jung, S., Mann, M., & Pouladi, M. A. (2020). Integrative analysis identifies key molecular signatures underlying neurodevelopmental deficits in fragile X syndrome. *Biological Psychiatry*, *88*, 500–511. https://doi.org/10.1016/j.biopsych.2020.05.005

Vasile, F., Dossi, E., & Rouach, N. (2017). Human astrocytes: Structure and functions in the healthy brain. *Brain Structure & Function*, *222*, 2017–2029. https://doi.org/10.1007/s00429-017-1383-5

Verkhratsky, A., Parpura, V., & Kettenmann, H. (2014). Encyclopedia of the neurological sciences. In M. J. Aminoff & R. B. Daroff (Eds.), *Encyclopedia of the neurological sciences* (2nd ed., pp. 290–295). Elsevier Inc. https://doi.org/10.1016/B978-0-12-385157-4.00582-0

Wen, T. H., Afroz, S., Reinhard, S. M., Palacios, A. R., Tapia, K., Binder, D. K., Razak, K. A., & Ethell, I. M. (2018). Genetic reduction of matrix metalloproteinase-9 promotes formation of perineuronal nets around parvalbumin-expressing interneurons and normalizes auditory cortex responses in developing Fmr1 knock-out mice. *Cereb Cortex*, *28*(11), 3951–3964. https://doi.org/10.1093/cercor/bhx258

Yepes, M. (2020). Urokinase-type plasminogen activator is a modulator of synaptic plasticity in the central nervous system: Implications for neurorepair in the ischemic brain. *Neural Regeneration Research*, *15*, 620–624. https://doi.org/10.4103/1673-5374.266904

How to cite this article: Peteri, U.-K., Pitkonen, J., de Toma, I., Nieminen, O., Utami, K. H., Strandin, T. M., Corcoran, P., Roybon, L., Vaheri, A., Ethell, I., Casarotto, P., Pouladi, M. A., & Castrén, M. L. (2021). Urokinase plasminogen activator mediates changes in human astrocytes modeling fragile X syndrome. *Glia*, *69*(12), 2947–2962. https://doi.org/10.1002/glia.24080